Self-assembled nanodomains of semi-fluorinated alkanes on phospholipid monolayers

Hiromichi Nakahara, Marie Pierre Krafft, Osamu Shibata

Self-Assembled Nanodomains of Semi-Fluorinated Alkanes on Phospholipid Monolayers

Hiromichi Nakahara,[a] Marie Pierre Krafft,*[,b] and Osamu Shibata*[,c]

[a] *Department of Industrial Pharmacy, Daiichi University of Pharmacy, 22-1 Tamagawa-cho, Minami-ku Fukuoka 815-8511, Japan,*
[b] *Institut Charles Sadron (CNRS), University of Strasbourg, 23 rue du Loess. 67034 Strasbourg, France,*
[c] *Department of Biophysical Chemistry, Graduate School of Pharmaceutical Sciences, Nagasaki International University; 2825-7 Huis Ten Bosch, Sasebo, Nagasaki 859-3298, Japan*

*Corresponding authors:
Osamu SHIBATA
Department of Biophysical Chemistry, Faculty of Pharmaceutical Sciences,
Nagasaki International University, 2825-7 Huis Ten Bosch, Sasebo, Nagasaki 859-3298, Japan
Tel: +81-956-20-5743
Fax: +81-956-20-5743
E-mail: wosamu@niu.ac.jp

Marie Pierre KRAFFT
Institut Charles Sadron (CNRS), University of Strasbourg, 23 rue du Loess 67034 Strasbourg, France
E-mail: krafft@unistra.fr

Running Title: Interaction of semi-fluorinated alkanes with DPPC films

Keywords: Semi-fluorinated alkane; Fluorocarbon-hydrocarbon diblock; DPPC; Surface micelle; Surface pressure; Surface potential; Fluorescence microscopy

ABSTRACT

Hypothesis

The incorporation of semi-fluorinated alkanes into phospholipid monolayers modulates their interfacial behavior and structural organization through fluorocarbon-hydrocarbon interactions. While prior studies demonstrated hierarchical self-assembly of a semi-fluorinated tetrablock in dipalmitoylphosphatidylcholine (DPPC) monolayers, it remains unclear how variations in the hydrocarbon chain length and molecular architecture of the semi-fluorinated alkane influence phase behavior and multilayer formation. We hypothesize that comparing diblocks and tetrablocks will reveal key structural determinants governing nanodomain formation and vertical stacking.

Experiments

We studied Langmuir monolayers composed of DPPC mixed with semi-fluorinated diblocks $C_{10}F_{21}C_mH_{2m+1}$ (*F*10*Hm*, *m* = 16 and 20) and tetrablocks $((C_{10}F_{21}CH_2)(C_mH_{2m+1})CH\text{-}CH(C_{10}F_{21}CH_2)(C_mH_{2m+1})$ (di(*F*10*Hm*), *m* = 16 and 20). Surface pressure-area and surface potential-area isotherms were recorded, and fluorescence and atomic force microscopies were employed to examine domain morphology. Additionally, compression-expansion cycles were performed to assess the stability of the observed assemblies.

Findings

All (*F*-alkyl)alkanes formed nanodomains at low surface pressures, which reorganized into vertically stacked multilayers upon compression. However, while di*(F*10*H*16) forms flower-like hierarchical structures at the phase boundary of DPPC, driven by chain-length compatibility and dipolar interactions, di(*F*10*H*20) shows more diffuse assemblies. We analyze the difference in assembling behavior between the two derivatives and highlight the critical role

of hydrocarbon segments' length and symmetry in governing vertical segregation and domain morphology, thus offering new insight into the design of responsive interfacial materials.

INTRODUCTION

Partially fluorinated alkanes, or semi-fluorinated alkanes, are unique amphiphilic molecules that exhibit self-organization at interfaces despite lacking conventional polar headgroups. These molecules spontaneously form stable monolayers and nanostructures due to the strong phase incompatibility between their perfluorinated and hydrocarbon segments[1-9]. In *FnHm* diblocks, the interaction between the perfluoroalkyl segment (*F*-chain) and the hydrogenated segment (*H*-chain) generates a CF_2−CH_2 dipole, which plays a crucial role in self-assembly[10]. This dipole, along with the repulsive dipole-dipole interactions at the chain termini, drives the formation of nanodomains (30−50 nm in diameter) at the air−water interface and on solid substrates[5, 6, 8, 9]. These nanodomains can assemble into quasi-crystalline 2D arrays on water surfaces, even at zero surface pressure[11, 12]. Surface potential and grazing incidence X-ray diffraction studies suggest that the *Hm* segments are in contact with water, while the *Fn* moieties orient toward air[5, 13-15]. The structural robustness of these monolayers is further demonstrated in covalently linked tetrablocks (di(*FnHm*)), which form highly stable films[16-18].

Fluorinated amphiphiles, including *FnHm* diblocks, have been explored for biomedical

applications[19], such as ophthalmology[20, 21] and intravascular oxygen delivery[22-29]. They also show promise in synthetic lung surfactant formulations, where their ability to reduce surface tension makes them relevant to respiratory therapies[30-32]. Prior studies have demonstrated the potential of perfluorocarbons in lung surfactant replacement[33-36]. Additionally, mixed monolayers of dipalmitoylphosphatidylcholine (DPPC) and semi-fluorinated amphiphiles have been studied in the context of surfactant replacement therapies[37].

Interactions between *FnHm* diblocks and phospholipids have revealed lateral and vertical phase separation in mixed monolayers[38-40]. At low surface pressure, *FnHm* nanodomains coexist with phospholipid monolayers, while further compression leads to the vertical displacement of these domains atop the phospholipid layer[39]. Recently, we demonstrated that monolayers of DPPC and the semi-fluorinated tetrablock di(*F*10*H*16) formed complex flower-like assemblies upon compression, localized near the liquid-expanded (LE) to liquid-condensed (LC) phase transition[41]. These unique structures appeared near the liquid-expanded (LE) to liquid-condensed (LC) phase transition, significantly altering the morphology of DPPC domains. The tetrablock acts as a linactant, accumulating at the LE/LC interface to modulate line tension. However, that prior study was limited to a single tetrablock molecule (di(*F*10*H*16)) and did not address how variations in molecular architecture affect vertical segregation and higher-order morphology. To fill this knowledge gap, the present study introduces a systematic

structural comparison between two types of amphiphiles, diblock (*F*10*Hm*) and tetrablock (di(*F*10*Hm*)), each designed with two different hydrocarbon chain lengths (*m* = 16 and 20). This allows us to evaluate the effects of molecular symmetry and chain-length compatibility on interfacial behavior. Notably, the inclusion of di(*F*10*H*20) represents a new molecular system not previously reported, enabling direct comparison with di(*F*10*H*16) and assessment of how small architectural differences lead to pronounced changes in self-assembly pathways, such as the presence or absence of flower-like hierarchical structures. This dual-axis design, which varies both molecular symmetry and chain length, offers a rational framework to investigate the underlying mechanisms of nanodomain formation, interfacial expulsion, and vertical stacking. Understanding these structure–function relationships is not only of fundamental interest for colloid and interface science but also offers insights relevant to nanostructured materials design and biomedical applications such as in microbubble stabilization[42]. Drawing parallels to protein-surfactant assemblies, such as keratin–surfactant complexes[43], we highlight how specific molecular features can be tuned to modulate self-assembly and interfacial functionality.

To elucidate the structure and formation mechanism of these flower-like assemblies, we investigate DPPC/*F*10*Hm* and DPPC/di(*F*10*Hm*) (*m* = 16 and 20) monolayers using surface pressure-area (π–A) isotherms, surface potential-area (ΔV–A) isotherms, fluorescence microscopy (FM), and Brewster angle microscopy (BAM). Langmuir-Blodgett (LB) films were also analyzed using atomic force microscopy (AFM) to characterize their morphology post-

transfer. The thermodynamic and structural properties of these novel 2D and 3D organizations are discussed in detail.

MATERIALS AND METHODS

Materials

The fluorocarbon-hydrocarbon diblocks (*F*10*Hm*) and tetrablocks (di(*F*10*Hm*)), with *m* = 16 or 20 (Fig. 1), were synthesized following established methodologies reported in the literature[16, 17, 44]. Purity levels exceeding 99% were confirmed through thin-layer chromatography (TLC), nuclear magnetic resonance (NMR) spectroscopy, elemental analysis, and matrix-assisted laser desorption/ionization time-of-flight (MALDI-TOF) mass spectrometry. These compounds possess chiral centers in their molecular structures; however, it was assumed that the products were obtained as racemic mixtures. 1,2-Dipalmitoyl-sn-glycero-3-phosphocholine (DPPC; >99%) and 1-palmitoyl-2-[6-[(7-nitro-2-1,3-benzoxadiazol-4-yl)amino]hexanoyl]-*sn*-glycero-3-phosphocholine (NBD-PC; >99%) were sourced from Avanti Polar Lipids (Alabaster, AL, USA). Chloroform (99.7%), utilized as the spreading solvent in Langmuir monolayer experiments, was procured from Kanto Chemical Co., Inc. (Tokyo, Japan). The subphase employed in all experiments consisted of thrice-distilled water, characterized by a surface tension of 72.0 mN m^{-1} at 298.2 K and an electrical resistivity of 18 MΩ·cm.

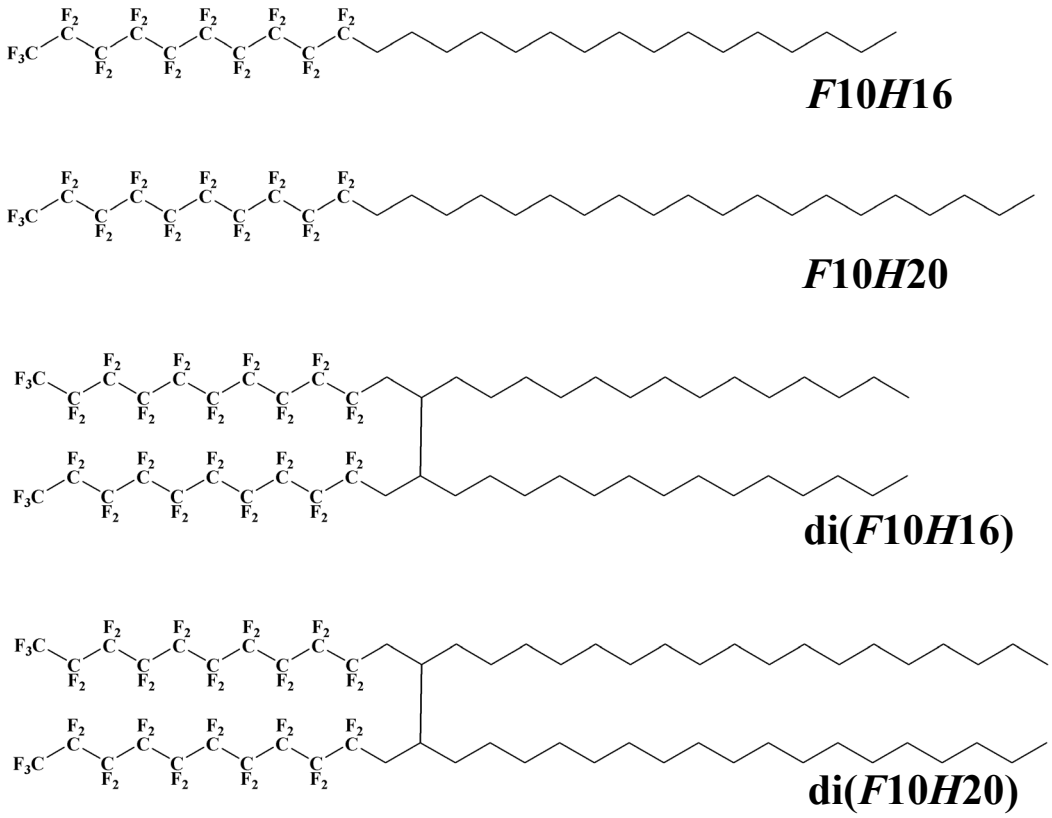

Fig. 1 Chemical structures of *F*10*H*16, *F*10*H*20, di(*F*10*H*16), and di(*F*10*H*20).

Methods

Isotherm measurements

To examine interfacial characteristics, Langmuir monolayers were studied under controlled temperature conditions (298.2 ± 0.1 K) by recording surface pressure (π) versus molecular area (A) isotherms and monitoring surface potential (ΔV). A combination of a KSV Minitrough and a KSV SPOT1 surface potential meter (KSV Instruments Ltd., Finland) was used. The surface pressure was measured via a Wilhelmy plate method utilizing a hydrophilic

filter paper strip (25 mm × 10 mm, periphery = 2.0 cm, e.g., Whatman Grade 541). Details regarding the experimental setup are available in prior studies[45, 46]. Stock solutions of *F*10*Hm*, di(*F*10*Hm*), and DPPC (1 mM) were prepared in chloroform. Twenty-five microliters of these solutions were carefully spread onto the air−water interface, followed by a solvent evaporation period of 15 min. Compression speeds varied from approximately 0.016 to 0.080 nm^2 $molecule^{-1}$ min^{-1}, and it was confirmed that this variation did not significantly alter the isotherm profiles. Consequently, a standardized compression/expansion speed of ~0.080 nm^2 $molecule^{-1}$ min^{-1} was adopted. The compressibility modulus (Cs^{-1}) was determined from the π–A isotherms using the equation: $Cs^{-1} = -A\left(\frac{\partial \pi}{\partial A}\right)_T$

The surface potential (ΔV) was measured concurrently with π during monolayer compression. A Kelvin probe system (KSV SPOT1, KSV Instruments Ltd.) positioned 1–2 mm above the interface recorded ΔV values, while a counter electrode remained submerged in the subphase. The instrument resolution was maintained at 1 mV.

Note that, in this study, the molecular area calculated from the isotherm is based on the assumption that all molecules are present at the air–water interface. Even though vertical expulsion and stacking may occur at high surface pressures, this averaged molecular area is intentionally used as a unified parameter for systematic comparison.

Fluorescence microscopy (FM)

To visualize monolayer morphology, the KSV Minitrough was mounted onto an Olympus

BX51WI fluorescence microscope (Tokyo, Japan), equipped with a 100 W mercury lamp (USH-1030L), a high-magnification objective lens (SLMPlan; 50×, working distance = 15 mm), and a 3CCD camera with an integrated control unit (IKTU51CU, Toshiba, Japan)[46, 47]. Prior to spreading, the stock solutions of the amphiphiles were mixed with 1 mol% of the NBD-PC fluorescence probe to enable imaging.

Atomic force microscopy (AFM)

Langmuir-Blodgett (LB) films were prepared using the KSV Minitrough. Freshly cleaved mica substrates (Okenshoji Co., Tokyo, Japan) were employed for vertical deposition. At predetermined surface pressures, films were transferred at a dipping rate of 5 mm min^{-1} while maintaining a constant temperature of 298.2 K. LB films with a deposition rate of ~1 were used in the experiments. AFM imaging was performed in tapping mode under ambient conditions (~298.2 K) using an SPA 400 atomic force microscope (Seiko Instruments Co., Chiba, Japan).

RESULTS

Isotherms of pure semi-fluorinated alkane di- and tetrablocks

The π–A and ΔV–A isotherms of monolayers formed by semi-fluorinated diblocks ($F10Hm$, m = 16, 20) and tetrablocks (di($F10Hm$)) at the air–water interface exhibited distinct features, reflecting differences in molecular architecture (Fig. 2). At large molecular areas (A > 0.40 nm^2 for diblocks and A > 0.75 nm^2 for tetrablocks), surface pressure remained low, indicating the presence of loosely packed molecules. Upon further compression, both systems exhibited a sharp rise in surface pressure, indicative of a phase transition from an expanded to a more condensed monolayer phase. The extrapolated molecular areas (A_0) for diblocks were ~0.35 nm^2, consistent with the cross-sectional area of F-alkyl chains (~0.30 nm^2)[1, 8], whereas those of tetrablocks (~0.65 nm^2) were approximately twice this value[18]. The collapse pressure (π^c) was consistently higher for diblocks than for tetrablocks, suggesting that the diblock molecules possess reduced conformational freedom and exhibit tighter molecular packing. The surface potential ΔV decreased with compression for all samples, reaching −900 ± 30 mV at the point of monolayer collapse. These negative values indicate the orientation of the perfluorinated chains toward the air phase, while the hydrocarbon segments remain in contact with water. Within each series, longer Hm chains resulted in more negative ΔV values, consistent with enhanced dipole alignment along the surface normal.

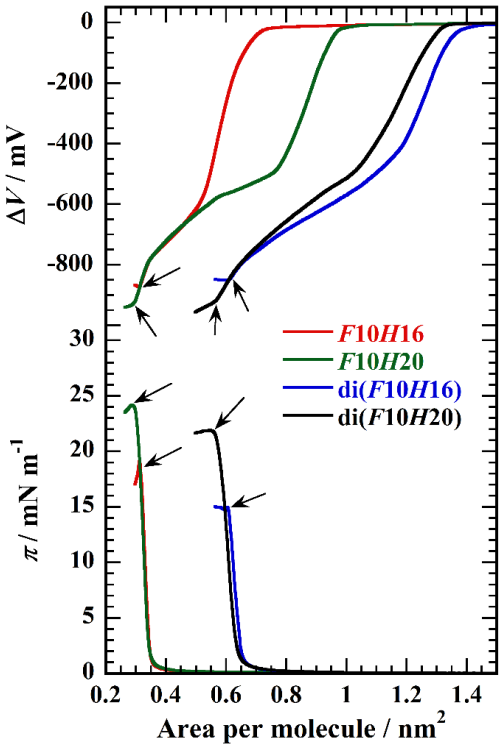

Figure 2. π–A and ΔV–A isotherms of $F10H16$, $F10H20$, di($F10H16$), and di($F10H20$) monolayers spread on water at 298.2 K.

Isotherms of di- and tetrablocks/DPPC mixed monolayers

The π–A and ΔV–A isotherms of monolayers composed of DPPC, semi-fluorinated di- and tetrablocks, and their binary mixtures are presented in Fig. 3 as a function of the mole fraction of the (*F*-alkyl)alkane block component ($X_{F\text{-AA}}$). Pure DPPC monolayers exhibit a first-order phase transition from the liquid-expanded (LE) to the liquid-condensed (LC) phase at approximately 12 mN m^{-1}, followed by monolayer collapse near 55 mN m^{-1}.

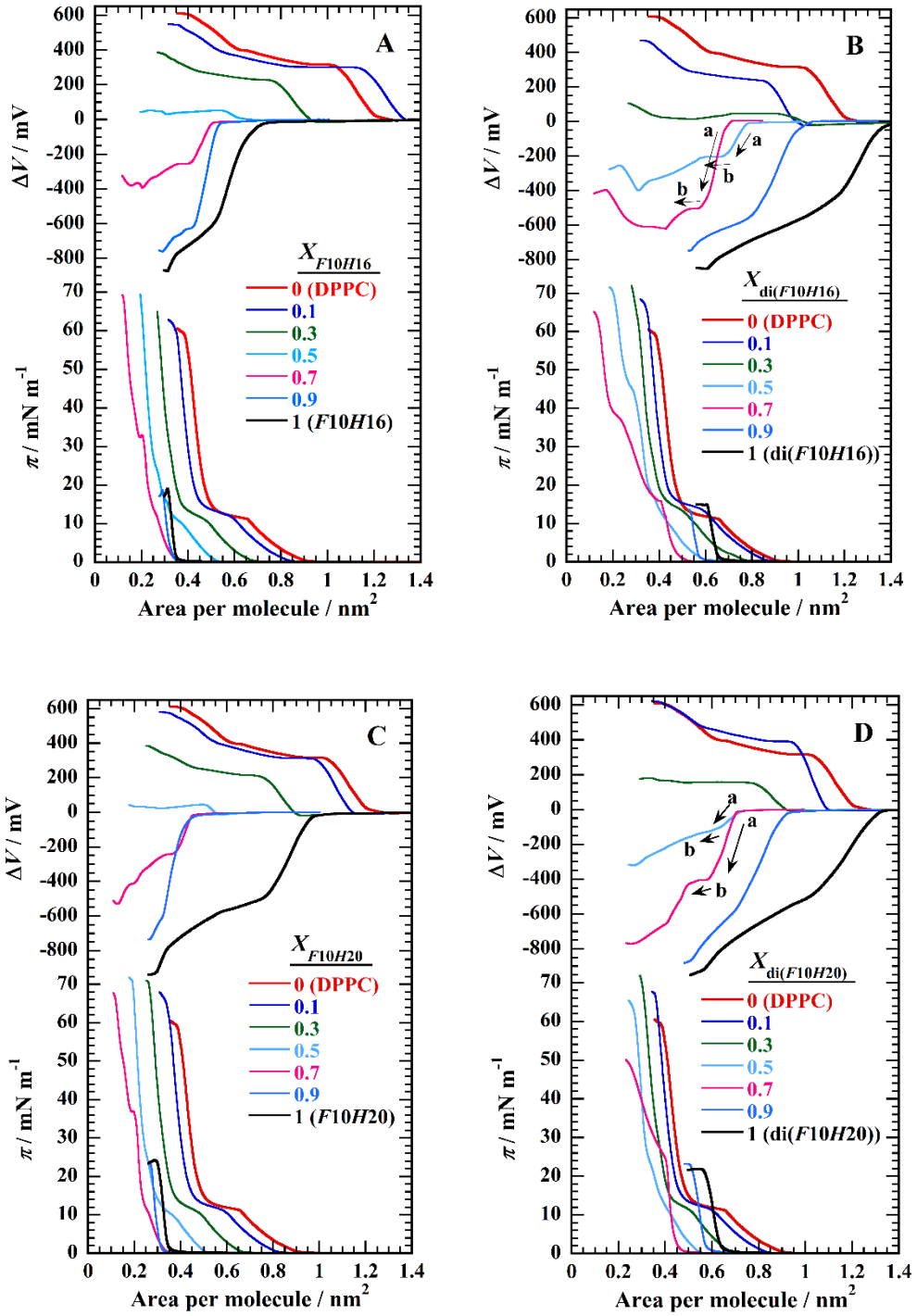

Figure 3. The π–A and ΔV–A isotherms of the two-component (A) DPPC/*F*10*H*16, (B) DPPC/di(*F*10*H*16), (C) DPPC/(*F*10*H*20) and (D) DPPC/di(*F*10*H*20) monolayers on water at 298.2 K.

In the binary monolayers, the isotherms shift to smaller molecular areas, which may suggest a partial incorporation and/or expulsion of the di- and tetrablock components at the interface.

While such reduction in area could preliminarily indicate molecular reorganization, including potential vertical stacking, further evidence from ΔV–A isotherms, FM, and AFM observations is necessary to support this hypothesis and is discussed in the following sections. For $X_{F\text{-AA}} \leq 0.7$, elevated collapse pressures (>60 mN m^{-1}) are maintained, suggesting a stabilizing effect of the (*F*-alkyl)alkane components within the mixed monolayers. The characteristic LE/LC transition plateau of DPPC becomes progressively less distinct with increasing $X_{F\text{-AA}}$, but remains detectable up to $X_{F\text{-AA}} = 0.7$; it is nearly absent at $X_{F\text{-AA}} = 0.9$. For $X_{F\text{-AA}} = 0.5$ and 0.7, additional inflection points appear in both π–A and ΔV–A isotherms, indicating structural rearrangements within the interfacial layer. The ΔV–A isotherm of DPPC alone exhibits a gradual increase in surface potential, reaching ~600 mV, with a plateau corresponding to the LE/LC transition region. In the mixed monolayers, ΔV transitions from positive to negative values as $X_{F\text{-AA}}$ increases. Notably, for $X_{F\text{-AA}} = 0.5$, the ΔV–A isotherms display non-monotonic behavior, indicative of competing molecular orientations at the interface.

Quantitative analyses of the expulsion of the (*F*-alkyl)alkanes from the DPPC interface

Figure 4 presents the mean molecular area (A) at a surface pressure of 5 mN m^{-1} as a function of $X_{F\text{-AA}}$ for DPPC/*F*10*H*16 and DPPC/di(*F*10*H*16) systems (Fig. 4A), and for DPPC/*F*10*H*20 and DPPC/di(*F*10*H*20) systems (Fig. 4B). In both systems, the experimentally

measured A values (solid symbols) lie below the ideal values (dashed lines) predicted by the additivity rule, indicating a negative deviation from ideal mixing behavior. This behavior shows that (*F*-alkyl)alkanes are partially expelled ("squeezed out") from the DPPC monolayer interface even at low surface pressure.

Figure 5 shows the loss ratio of (*F*-alkyl)alkanes at 5 mN m^{-1}, calculated as $(A^{\text{ideal}} - A)/A_{F\text{-AA}}\, X_{F\text{-AA}}$, is plotted against $X_{F\text{-AA}}$. Across the entire $X_{F\text{-AA}}$ range, all (*F*-alkyl)alkanes species exhibit partial expulsion from the DPPC monolayers, even at a surface pressure of 5 mN m^{-1}. This surface pressure is well below the collapse pressure (π^{c}) of the pure (*F*-alkyl)alkane monolayers. At $X_{F\text{-AA}}$ = 0.9, the loss ratio remains relatively low, indicating minimal expulsion under these conditions. In the binary systems with $X_{F\text{-AA}}$ between 0.1 and 0.7, the expulsion of (*F*-alkyl)alkanes is significantly enhanced. Notably, in the range of $X_{F\text{-AA}}$ = 0.3–0.7, approximately 50–70% of the (*F*-alkyl)alkane molecules are excluded from the interface and are believed to be displaced onto the upper surface of the DPPC monolayer. Figure S1 in the Supplementary material complements this by showing the DPPC-based loss ratio at 5 mN m^{-1}; $(A^{\text{ideal}} - A)/A_{\text{DPPC}}\,(1–X_{F\text{-AA}})$. At high *F*-alkyl fractions ($X_{F\text{-AA}} \geq 0.7$), the loss ratio exceeds 100 %, which is far from indicating unphysical over-expulsion of DPPC, provides strong indirect evidence that DPPC remains at the interface while *F*-alkane is selectively expelled. Here, the vanishingly small denominator of $A_{\text{DPPC}}\,(1–X_{F\text{-AA}})$ mathematically amplifies the contrast between negligible DPPC loss and substantial *F*-alkane loss.

A comparison between the diblock and tetrablock compounds reveals a clear difference in their expulsion behavior from the DPPC monolayers. Notably, compounds containing longer hydrocarbon chains (*H*20) exhibit a higher propensity to be expelled, regardless of their molecular architecture. This trend is particularly evident in DPPC-rich mixtures ($X_{F\text{-AA}}$ = 0.1–0.7). In this range, *F*10*H*20 shows the highest loss ratio, reaching nearly 75% at $X_{F\text{-AA}}$ = 0.3–0.5, suggesting substantial incompatibility with the DPPC matrix. The expulsion of di(*F*10*H*20) is also pronounced, although less so than its diblock counterpart. On the other hand, *F*10*H*16 and di(*F*10*H*16) exhibit relatively moderate loss ratios in the same region, implying better interfacial compatibility with DPPC. These differences are likely due to the combined effects of molecular rigidity, chain length, and packing constraints, which influence the insertion and retention of the fluorinated molecules within the DPPC monolayer. The findings indicate that both chain length and molecular symmetry significantly affect interfacial behavior, particularly under conditions where DPPC dominates the monolayer composition.

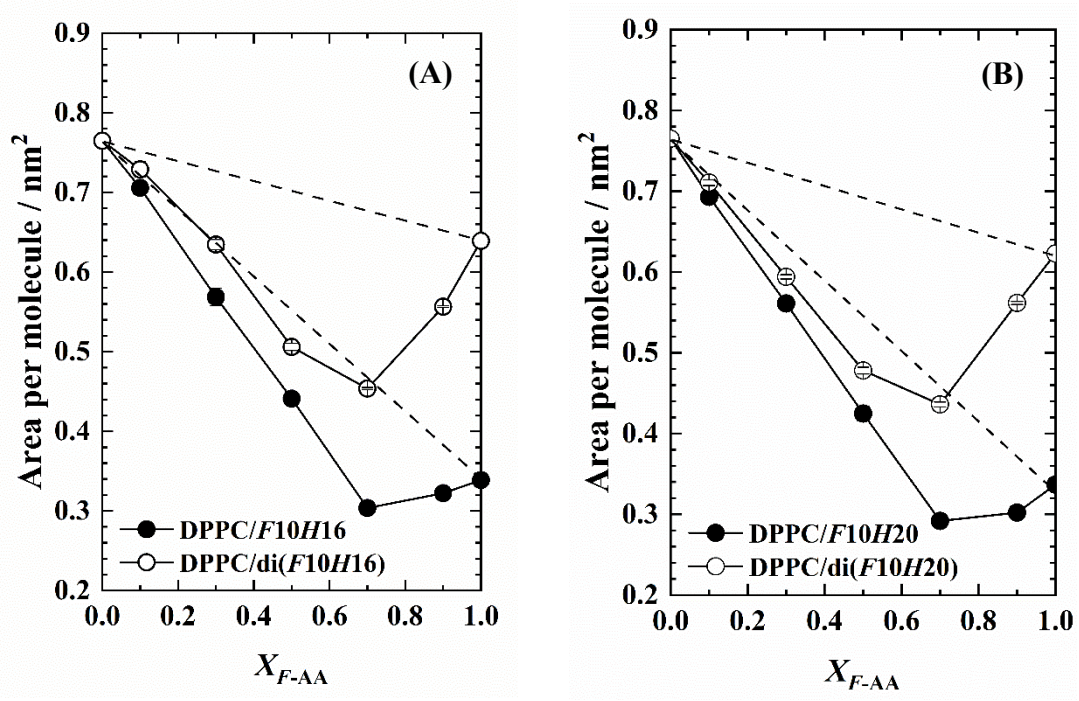

Figure 4. Mean molecular area of (A) the DPPC/*F*10*H*16 and DPPC/di(*F*10*H*16), and (B) the DPPC/*F*10*H*20 and DPPC/di(*F*10*H*20) monolayers as a function of $X_{F\text{-AA}}$ at 5 mN m^{-1}. The dashed lines were calculated by assuming the additivity rule; the solid points represent experimental values.

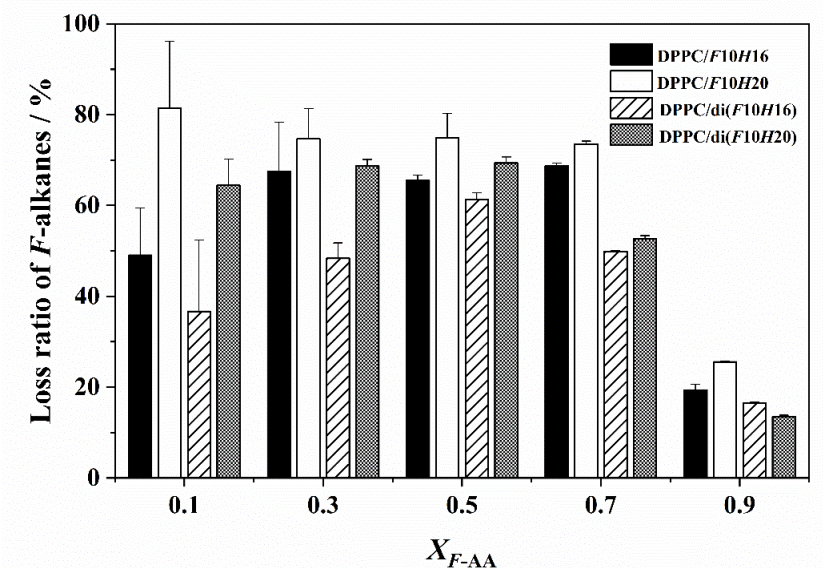

Figure 5. The ratio of (*F*-alkyl)alkane di- and tetrablocks excluded from the surface monolayer for the binary systems as a function of $X_{F\text{-AA}}$ at 5 mN m^{-1} under the assumptions of an ideal mixing or immiscible interaction between the two components and of no elimination of DPPC from the interface on lateral compression.

Vertical stacking of di(*F*10*H*16) and di(*F*10*H*20) on DPPC monolayers

Figure 6 shows the π–A, ΔV–A, and Cs^{-1}–A isotherms of DPPC/di(*F*10*H*16) and DPPC/di(*F*10*H*20) monolayers at $X_{di(F10Hm)} = 0.3$. For the DPPC/di(*F*10*H*16) system (Fig. 6A), distinct inflection points in both ΔV–A and Cs^{-1}–A isotherms are observed at defined molecular areas, suggesting stepwise structural reorganizations during compression. At larger molecular areas, fluorinated amphiphiles are initially dispersed within the monolayer (Scheme 1a). As compression proceeds, vertical displacement of di(*F*10*H*16) above the DPPC monolayer occurs around $A \approx 0.71$ nm^2 (Scheme 1b), as evidenced by a marked negative shift in ΔV. This decrease in surface potential reflects the reorientation of molecular dipoles, particularly the upward movement of the fluorocarbon segments toward the air phase, thereby reducing the net dipole moment normal to the interface. Such a shift strongly supports the notion of vertical segregation and stacking. Continued compression results in a second change in the ΔV slope, indicative of further molecular stacking or reorganization (Scheme 1c). A third transition near $A \approx 0.48$ nm^2 and $\pi \approx 12$ mN m^{-1} corresponds to the LE/LC phase transition of DPPC (Scheme 1d). These inflection points were each measured independently three times, and all replicate curves are overlaid in Fig. S2 to visually demonstrate the variability and reproducibility of the isotherms. In contrast, the DPPC/di(*F*10*H*20) monolayer (Fig. 6B) displays a similar inflection in the π–A isotherm near the LE/LC transition (~12 mN m^{-1}). However, both the ΔV–A and Cs^{-1}–A profiles

are smoother and do not exhibit distinct slope changes, suggesting a more continuous and less stepwise reorganization.

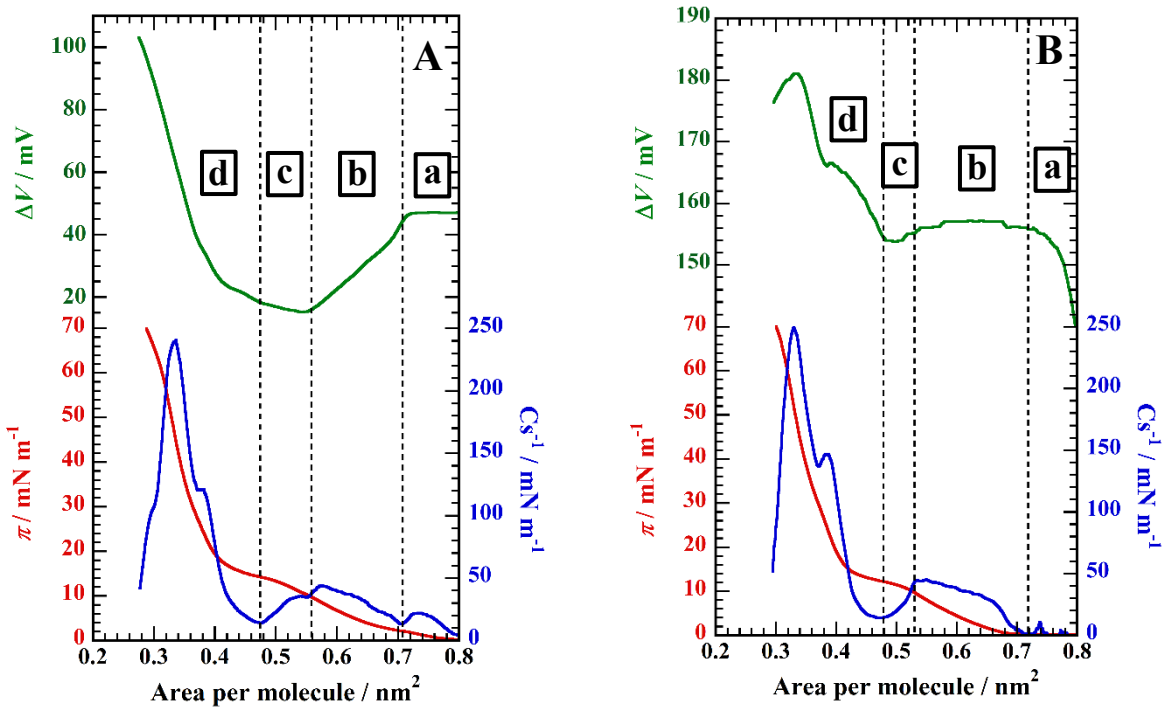

Figure 6. The π–A, Cs^{-1}–A, and ΔV–A isotherms of the two-component (A) DPPC/di(*F*10*H*16) and (B) DPPC/di(*F*10*H*20) monolayers at $X_{F\text{-AA}} = 0.3$ on water at 298.2 K. Enclosed letters a–d correspond to Scheme 1a–d.

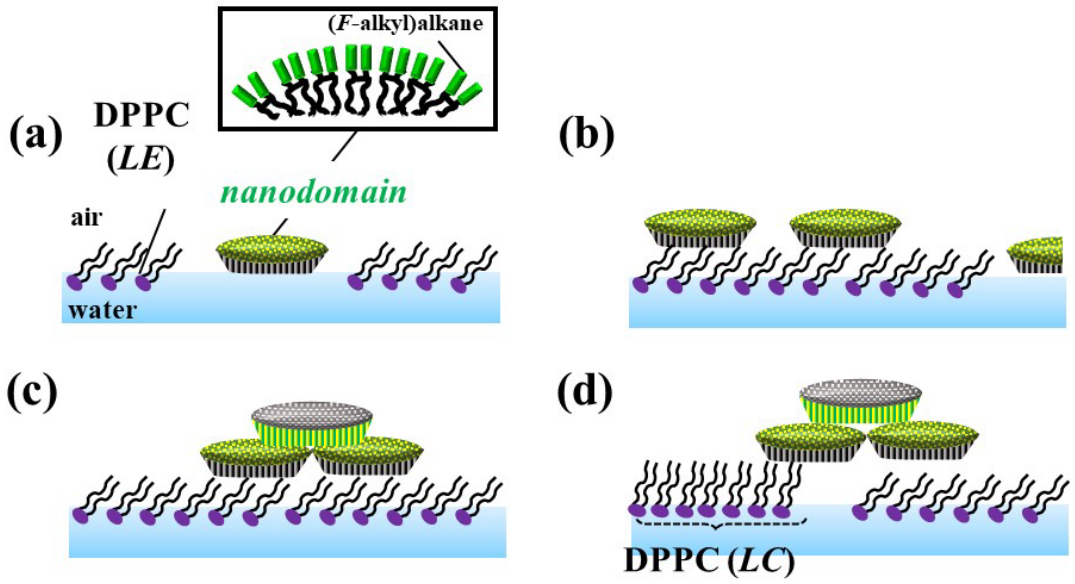

Scheme 1. Vertical stacking of surface micelles of *F*10*H*16 and di(*F*10*H*16) on the top of DPPC monolayers during lateral compression.

In situ morphological analyses of DPPC/(*F*-alkyl)alkane monolayers

Fluorescence microscopy (FM) imaging of DPPC monolayers revealed distinct pressure-dependent morphological features that varied with the presence and molecular type of (*F*-alkyl)alkane additives. Pure DPPC monolayers exhibited characteristic phase-separated morphologies above ~12 mN m^{-1}, with bright regions corresponding to the LE phase and dark, bean-shaped domains representing the LC phase that expanded progressively upon compression. In the DPPC/*F*10*Hm* (diblock) systems, FM images showed a complete disappearance of the LC domains across the entire pressure range (Figs. S3 and S4), indicating substantial disruption of DPPC domain formation by the incorporated diblocks. The DPPC/di(*F*10*H*16) monolayers at $X = 0.3$ exhibited a notable pressure-dependent morphological evolution, as visualized in Figs. 7 and S3C. Below 12 mN m^{-1}, the images appeared uniformly bright, indicating a homogeneous LE phase. Above this threshold, large "flower-like" microstructures emerged, characterized by bright central cores, radially extending arms, and terminal bright spots. These hierarchical structures were most prominent between 15 and 50 mN m^{-1} (Fig. S5). Upon further compression to 55 mN m^{-1}, most LE domains transitioned into the LC phase.

In contrast, the DPPC/di(*F*10*H*20) monolayers exhibited uniformly bright FM images throughout the entire pressure range (Figs. 7 and S6), with no indication of flower-like or radially organized structures, even at intermediate and high mole fractions ($X_{F\text{-AA}}$ = 0.5 and 0.7, see Fig. S6D,E). Similarly, the DPPC/*F*10*H*20 diblock systems displayed uniform brightness across all pressures (Fig. S4B), consistent with enhanced lateral miscibility and a lack of pressure-induced morphological transformations.

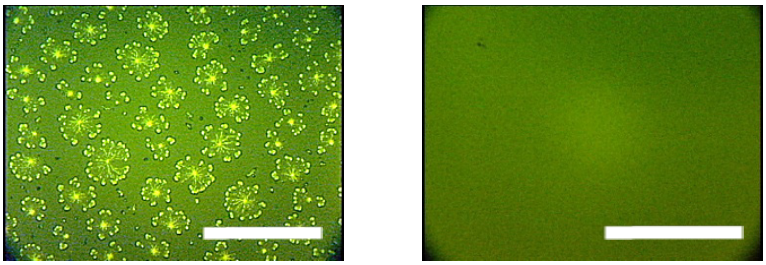

Figure 7. FM images of (A) DPPC/di(*F*10*H*16) and (B) DPPC/di(*F*10*H*20) monolayers for $X_{\text{di}(F10H16)}$ = 0.3 at 35 mN m^{-1} on water at 298.2 K. The monolayers contained 1 mol% Fluorescent probe (NBD-PC). The scale bar in the lower right represents 100 μm.

AFM topographies of binary monolayers

Langmuir–Blodgett (LB) films of DPPC/diblock and DPPC/tetrablock mixtures at X = 0.3 were transferred onto mica substrates and imaged using atomic force microscopy (AFM) (Fig. 8). In the DPPC/diblock systems, circular nanodomains (~40 nm in diameter) were observed on the LC regions of the DPPC monolayers, with measured heights of ~2.5 nm for *F*10*H*16 and ~2.8 nm for *F*10*H*20. These observed heights are lower than the estimated full

molecular lengths (3.7–4.2 nm), suggesting molecular tilting or bending at the CH_2–CF_2 junction. Compared to the surface density in pure diblock films (Fig. S7), the nanodomains in DPPC/diblock films appeared more sparsely and heterogeneously distributed. In the DPPC/di(*F*10*H*16) films, AFM imaging revealed prominent flower-like structures exhibiting radially protruding features with height differences of up to ~2.0 nm relative to the adjacent LC domains. DPPC/di(*F*10*H*20) films exhibited compact, circular nanodomains (~0.8–1.2 nm in height above the LC phase), which are significantly shorter than the estimated molecular length (~4.2 nm)[8]. This discrepancy likely reflects molecular tilting or folding at the CH_2–CF_2 junction, resulting in partial submersion of the *H*20 segments within the DPPC matrix or lateral orientation at the interface. By contrast, the DPPC/di(*F*1*0*H20) systems do not indicate extended or hierarchical flower-like morphology. In both tetrablock-containing systems, the nanodomains preferentially localized to the LE regions rather than the LC domains. This spatial distribution likely reflects favorable interactions between the hydrocarbon (*Hm*) segments of the tetrablocks and the more disordered hydrophobic chains of DPPC in the LE phase.

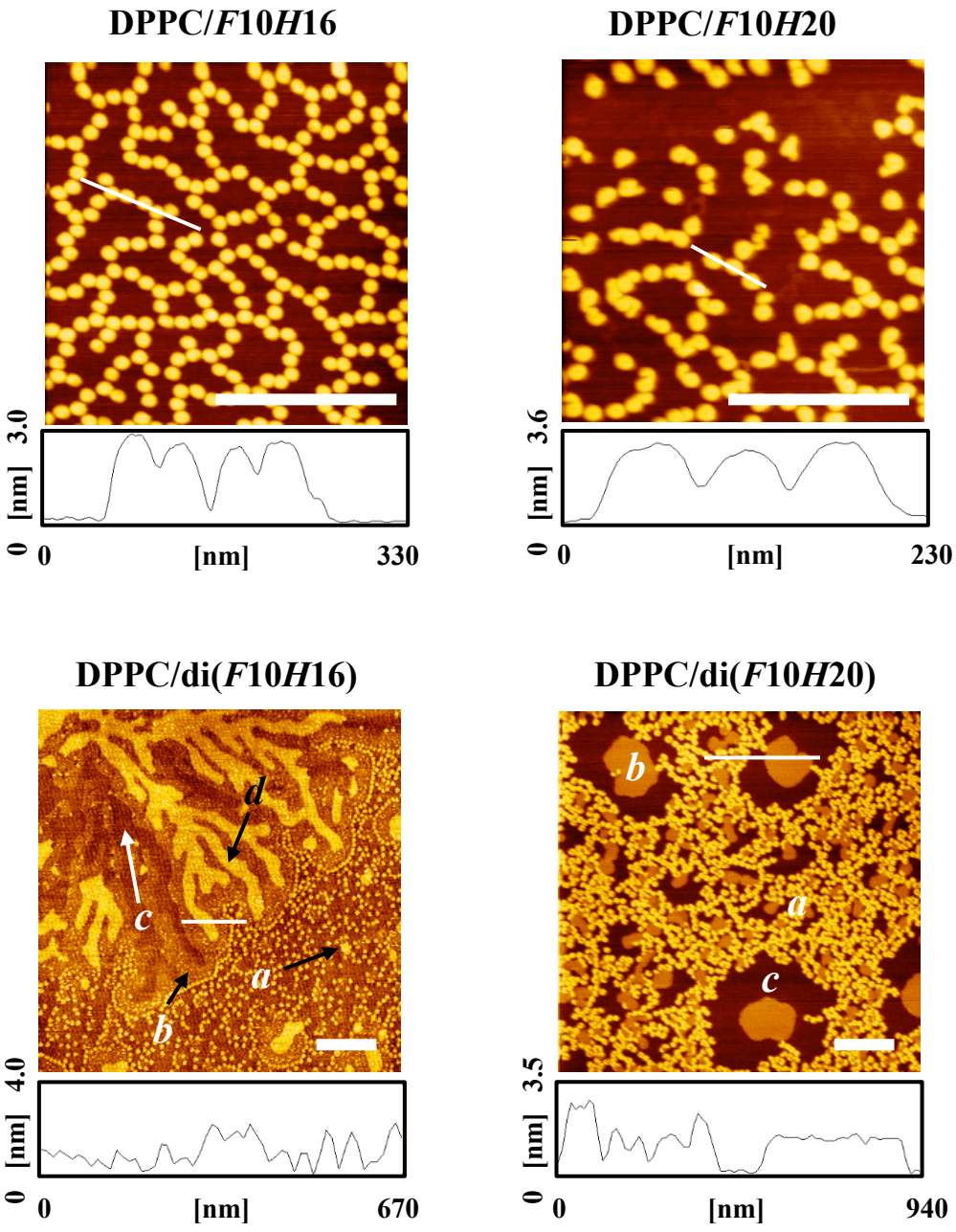

Figure 8. AFM topographic images of the binary DPPC/(*F*-alkyl)alkane monolayers ($X_{F\text{-AA}}$ = 0.3) transferred at 5 (for DPPC/di(*F*10*H*16)) and 25 mN m^{-1} (for the others)) on mica. The cross-sectional profiles along the scanning line (white) are provided below each image. The scale bars in the lower right represent 500 nm. The labels (*a*–*d*) correspond to the following features observed in the AFM images: (*a*) nanodomains excluded from the DPPC LC phase, (*b*) LC phase regions of DPPC, (*c*) LE phase regions of DPPC, (*d*) flower-like protrusions (finger-like moieties) characteristic of the DPPC/di(*F*10*H*16) system.

DISCUSSION

The compression-induced increase in surface pressure (π), along with the difference in limiting molecular area (A_0) between diblock and tetrablock amphiphiles, reflects distinct molecular packing behavior arising from their fluorocarbon-hydrocarbon architecture[48, 49]. This architecture plays a central role in dictating both lateral organization and monolayer stability[50]. Notably, diblocks exhibit higher collapse pressure (π^c), suggesting tighter packing and reduced conformational freedom compared to tetrablocks. In contrast, the more flexible tetrablock architecture compromises packing efficiency, leading to lower π^c values. These observations are consistent with surface potential (ΔV) measurements: strongly negative ΔV at collapse reflects an upright molecular orientation, with perfluorinated segments facing air and hydrocarbon chains directed toward the subphase[51]. Furthermore, increasing hydrocarbon chain length (*Hm*) leads to more negative ΔV values, likely due to enhanced dipole alignment and deeper insertion into the subphase. In mixed systems with DPPC, the progressive suppression of the LE/LC transition plateau and the appearance of multiple inflection points in the isotherms point to phase separation and interfacial restructuring. The non-monotonic ΔV–A behavior, especially at $X_{F\text{–}AA} > 0.5$, indicates competing molecular orientations. Tetrablocks induce more substantial changes than diblocks, highlighting their stronger and more disruptive interactions with the phospholipid matrix [52].

Unlike prior studies reporting lateral phase separation in DPPC monolayers with non-

fluorinated amphiphiles (e.g., tetrazine and glycyrrhizin derivatives)[45-47], our findings reveal a distinctly vertical segregation mechanism. This behavior is attributed to the asymmetric molecular architecture of the fluorinated amphiphiles, where immiscibility between the fluorocarbon and hydrocarbon segments drives directional partitioning. The appearance of stepwise plateaus and ΔV reductions in the isotherms supports the notion that tetrablocks migrate to the top of the DPPC monolayer upon compression. These findings emphasize the critical influence of fluorinated molecular design on interfacial self-assembly, offering a structural basis for developing amphiphilic systems with tailored stacking behavior.

The negative deviation of experimental molecular areas (*A*) from the ideal mixing line (Fig. 4) suggests limited miscibility between (*F*-alkyl)alkanes and DPPC at the air–water interface. Additionally, the low collapse pressure (~20 mN m^{-1}), which is less than half that of DPPC (~45 mN m^{-1}), reflects their reduced interfacial stability and tendency for selective expulsion under compression. This selective migration is likely driven by favorable van der Waals interactions between the *H*-chains of the fluorinated compounds and the hydrocarbon tails of DPPC, which are energetically more favorable than interactions with water. Taken together, these results are consistent with prior observations of fluorinated nanodomain displacement and reinforce the vertical phase separation model[41]. Interestingly, both *H*16- and *H*20-based systems show similar deviations from ideal mixing, implying that chain-length variation exerts minimal effect on the expulsion behavior under the current conditions. Upon

compression, expelled (*F*-alkyl)alkane molecules migrate to the upper surfaces of the DPPC layer ("squeezing-out"), thereby decreasing the average molecular area at the interface. This observation is consistent with previous findings showing that even minor disparities in chain length can significantly alter the mechanical properties of DPPC-based membranes[53]. The presumption that DPPC remains interfacially anchored is supported by its known strong interfacial activity. Moreover, the low loss ratio at $X_{F\text{–AA}} = 0.9$ (Fig. 5) indicates insufficient hydrocarbon content to stabilize *Hm* segments at low DPPC concentrations. In contrast, DPPC-rich systems facilitate greater upward migration of fluorinated compounds. Because this selective expulsion occurs well below collapse pressures (5 mN m^{-1}), it cannot be attributed to collapse-induced effects. Instead, these findings support the view that dipolar interactions and interfacial compatibility, rather than mechanical compression alone, dictate vertical segregation behavior. This insight highlights the critical role of molecular design in engineering hierarchical interfaces.

The stepwise changes observed in the isotherms of the DPPC/di(*F*10*H*16) monolayer (see Scheme 1a–d) provide clear evidence for vertical reorganization process of the fluorinated amphiphile. At large molecular areas, di(*F*10*H*16) molecules initially reside at the air–water interface. Upon compression, they migrate vertically to form a layer atop the DPPC monolayer (Scheme 1b), followed by stacking (Scheme 1c) and reorientation that coincides with the LE to LC phase transition of DPPC (Scheme 1d). These observations suggest a strong coupling

between lateral phase behavior and vertical assembly in the di(*F*10*H*16) system.

In contrast, the Δ*V–A* isotherm for the DPPC/di(*F*10*H*20) system (Fig. 6B) lacks abrupt slope changes, indicating a more diffuse or incomplete vertical stacking process. This difference can be attributed to the longer *H*20 segment, which likely imparts greater conformational flexibility and enhances miscibility with DPPC. While longer hydrocarbon chains generally promote packing via van der Waals forces, previous studies have shown that excessive chain length introduces entropic penalties, particularly in disordered or mixed systems[54, 55]. This entropy-driven flexibility counteracts the stabilizing effects of van der Waals interactions, favoring mixing and thereby inhibiting vertical segregation. These findings highlight how small architectural variations, such as chain length, can dramatically impact interfacial assembly dynamics and structural outcomes.

Cyclic isotherm measurements further support the vertical reorganization model. The high reproducibility across compression–expansion cycles indicates a robust and resilient DPPC/di(*F*10*H*16) interface (see Fig. S8). Notably, the hysteresis observed during expansion, including a distinct kink, indicates reversible migration of fluorinated nanodomains back to the air–water interface. This behavior reflects strong vertical interactions and a capacity for dynamic reconfiguration. The irreversible changes seen in the first cycle, followed by consistent behavior thereafter, suggest a curing or annealing process that promotes nanodomain ordering and stabilizes the interface. In contrast, the DPPC/di(*F*10*H*20) system exhibited much weaker

hysteresis, with nearly overlapping compression–expansion isotherms and no obvious kinks in the Δ*V*–*A* profiles, indicating minimal vertical rearrangement or nanodomain restructuring. This difference likely stems from the enhanced lateral miscibility and conformational flexibility associated with the longer *H*20 chains, which suppresses hierarchical stacking behavior. These findings underscore the potential of fluorinated tetrablocks in applications where robust, reconfigurable interfacial architectures are essential, such as lung surfactant analogs or interfacial drug delivery platforms. Remarkably, such reversible, thixotropic behavior, which is typically attributed to complex macromolecular surfactants, is here achieved using simple, low-molecular-weight semifluorinated amphiphiles. This highlights how precise molecular design can impart biological-like responsiveness to fully synthetic materials. The reproducibility and tunability of nanostructure formation in the DPPC/di(*F*10*H*16) system affirm the feasibility of engineering functional, adaptive interfacial architectures using small molecules.

These structural insights are supported by FM observation (Fig. 7). The DPPC/di(*F*10*H*16) monolayers exhibit distinct flower-like microstructures, confirming the formation of stable, spatially organized nanodomains. In contrast, DPPC/di(*F*10*H*20) monolayers display uniform, featureless bright regions, indicative of disordered or fully mixed assemblies. As illustrated in Scheme 2, these contrasting morphologies can be attributed to differences in molecular architecture. In the di(*F*10*H*16) system, the *H*16 segments closely match the C16 tails of DPPC, facilitating optimal van der Waals interactions, tighter lateral

packing, and even interdigitated-like arrangements. This structural proximity enhances oleophobic repulsion between hydrocarbon and fluorocarbon segments, promoting accumulation of di(*F*10*H*16) at LE/LC boundaries and leading to vertical stacking and flower-like patterns. In contrast, the longer *H*20 chains in di(*F*10*H*20) increase the spatial gap between fluorocarbon blocks and DPPC chains, weakening oleophobic interactions and increasing miscibility. As a result, ordered microstructure formation is suppressed. This observation aligns with previous studies showing that chain-length mismatch weakens lateral cohesion and enhances mixing in lipid environments[56]. These results emphasize that interfacial organization is highly sensitive to molecular symmetry and hydrocarbon chain compatibility, and that small architectural modifications can markedly impact nanostructure formation at the air–water interface.

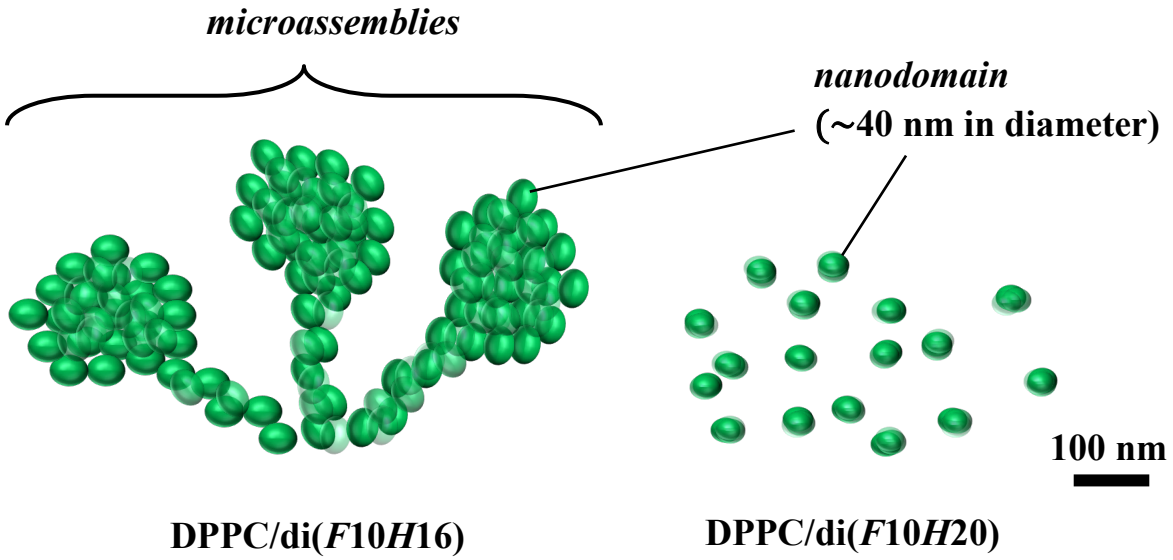

Scheme 2 Schematic representation of the hierarchical self-assembly behavior of fluorinated amphiphiles in DPPC monolayers. In the DPPC/di(*F*10*H*16) system (left), nanodomains (green circles, ~40 nm in diameter) coalesce into vertically and laterally ordered flower-like microassemblies due to favorable chain-length matching and dipolar repulsion effects. In contrast, the DPPC/di(*F*10*H*20) system (right) shows dispersed nanodomains (green circles) lacking sufficient stability and cohesion, resulting in the absence of higher-order structures. The scale bar in the lower right represents 100 nm.

In DPPC/di(*F*10*H*16) systems, the emergence of flower-like superstructures correlates closely with the LE/LC transition pressure of DPPC, suggesting that phase behavior of the phospholipid matrix governs structural rearrangement. These patterns likely result from nanodomain fusion, interfacial energy minimization, and line tension reduction. Bright FM signals within the flower-like domains suggest preferential accumulation of the fluorescent probe in hydrocarbon-rich regions, supporting a stabilizing role for interactions between DPPC tails and the *Hm* chains of di(*F*10*H*16). The observed radial symmetry and pattern regularity point to a self-limiting growth mechanism regulated by dipole–dipole repulsions and line

tension gradients. Similar morphologies have been associated with the incorporation of insoluble fluorinated amphiphiles into DPPC LC domains[57]. Notably, these stacked nanodomains may act as 2D surfactants, or "linactants"[41, 58, 59], preferentially adsorbing at phase boundaries to reduce interfacial energy−an interpretation supported by previous BAM studies[57].

In contrast, the DPPC/di(*F*10*H*20) system shows no such structural features, underscoring the impact of hydrocarbon chain length. The extended *H*20 segment likely increases DPPC miscibility and steric hindrance, thereby suppressing vertical segregation and aggregation. Nevertheless, AFM imaging reveals partial vertical segregation, highlighting persistent fluorocarbon–hydrocarbon immiscibility. The consistent size and shape of the nanodomains in both systems also point to their intrinsic mechanical robustness[18]. Notably, flower-like assemblies form only at a mole fraction of $X = 0.3$, suggesting that a critical balance between chain-length matching and phase immiscibility is required for pattern formation. This dynamic restructuring underscores how small differences in molecular architecture can dictate macroscale morphological outcomes. Finally, the preferential accumulation of (*F*-alkyl)alkanes at the air–lipid and air–water interfaces[41, 59] suggests their utility as interfacial carriers or solubilizers for hydrophobic agents. The ability of di(*F*10*H*16) to drive significant domain remodeling without polar headgroups highlights the dominant role of physical forces—van der Waals interactions, dipolar effects, and steric packing—in controlling interfacial behavior.

These findings position fluorinated tetrablocks as powerful modulators of lipid organization, with promising applications in adaptive surfactant systems and lipid-based drug delivery platforms.

CONCLUSIONS

This study elucidates the hierarchical self-assembly behavior of semi-fluorinated alkanes (*F*10*Hm* and di(*F*10*Hm*), *m* = 16 and 20) in DPPC monolayers at the air−water interface. These amphiphiles formed nanodomains at low surface pressures and exhibited vertical stacking upon compression. Surface potential and fluorescence microscopy measurements confirmed a preferential orientation, with fluorocarbon segments directed toward air and hydrocarbon chains facing the aqueous subphase. Beyond previous reports of stacked fluorinated nanodomains[41], we establish a well-defined vertical segregation mechanism, controlled by molecular symmetry and chain-length matching. Only di(*F*10*H*16) produces ordered flower-like assemblies, whereas di(*F*10*H*20) forms diffuse structures, underscoring the decisive role of chain-length compatibility. These results demonstrate that even subtle architectural changes can reshape nanoscale organization at fluid interfaces. Unlike protein−surfactant complexes such as keratin − ionic surfactant assemblies[43], which rely on electrostatic and hydrogen-bonding interactions, our system demonstrates that nonpolar amphiphiles can achieve robust interfacial structuring purely through dipole–dipole and van der

Waals forces. This distinguishes semi-fluorinated alkanes from protein–surfactant complexes and highlights their versatility as tunable building blocks for interfacial engineering. The reproducibility and reversibility of nanostructure formation, including thixotropic behavior and surface tension hysteresis, further underscore their potential in adaptive interfacial materials. These insights offer practical design principles for the next generation of functional surfactants. Potential applications include pulmonary surfactant therapy, drug delivery, and microbubble stabilization, where both structural robustness and dynamic responsiveness are essential. While precise micrometer-scale patterning remains to be achieved, the demonstrated ability to selectively control assembly via molecular parameters represents a significant step forward. Looking ahead, introducing responsive moieties and exploring additional architectural variations will allow fine-tuning of assembly dynamics and functional diversification. Moreover, direct structural characterization using reflectivity techniques (e.g., XRR, NR) will be crucial for validating and quantifying the multilayered architectures proposed here.

ACKNOWLEDGEMENTS

This research was funded by a Grant-in-Aid for Scientific Research (C) 23K06076 from the Japan Society for the Promotion of Science (JSPS).

Declaration of Interests

The authors declare that they have no known competing financial interests or personal relationships that could have appeared to influence the work reported in this paper.

Funding Sources

This research was supported by a Grant-in-Aid for Scientific Research (C) (Grant No. 23K06076) from the Japan Society for the Promotion of Science (JSPS).

Data Availability Statement

The data that support the findings of this study are available from the corresponding author upon reasonable request.

Supplementary Material

Supplementary material, including additional experimental details, figures, and datasets, is available in a separate file accompanying this manuscript.

References

[1] G.L. Gaines, Jr., Surface activity of semifluorinated alkanes: F(CF2)m(CH2)nH, Langmuir 7(12) (1991) 3054-3056.

[2] M. Li, A.A. Acero, Z. Huang, S.A. Rice, Formation of an ordered Langmuir monolayer by a non-polar chain molecule, Nature 367(6459) (1994) 151-153.

[3] Z. Huang, A.A. Acero, N. Lei, S.A. Rice, Z. Zhang, M.L. Schlossman, Structural studies of semifluorinated hydrocarbon monolayers at the air/water interface, J. Chem. Soc. Faraday Trans. 92(4) (1996) 545-552.

[4] A.E. Abed, F.M. C., H. M., G. F., B. J., P. and Peretti, Molecular Orientation in a Semi-Fluorinated Alkane Monolayer Spread at the Air-Water Interface, Molec. Cryst. Liq. Cryst. 329(1) (1999) 283-292.

[5] M. Maaloum, P. Muller, M.P. Krafft, Monodisperse Surface Micelles of Nonpolar Amphiphiles in Langmuir Monolayers, Angew. Chem. Int. Ed. 41(22) (2002) 4331-4334.

[6] P. Fontaine, M. Goldmann, P. Muller, M.-C. Fauré, O. Konovalov, M.P. Krafft, Direct evidence for highly organized networks of circular surface micelles of surfactant at the air−water interface, J. Am. Chem. Soc. 127(2) (2005) 512-513.

[7] M. Broniatowski, P. Dynarowicz-Łątka, Semifluorinated alkanes — Primitive surfactants of fascinating properties, Adv. Colloid Interf. Sci. 138(2) (2008) 63-83.
[8] M.P. Krafft, J.G. Riess, Chemistry, physical chemistry, and uses of molecular fluorocarbon--hydrocarbon diblocks, triblocks, and related compounds--unique "apolar" components for self-assembled colloid and interface engineering, Chem. Rev. 109(5) (2009) 1714-1792.
[9] M.P. Krafft, Large organized surface domains self-assembled from nonpolar amphiphiles, Acc. Chem. Res. 45(4) (2012) 514-524.
[10] A.N. Semenov, A. González-Pérez, M.P. Krafft, J.-F. Legrand, Theory of Surface Micelles of Semifluorinated Alkanes, Langmuir 22(21) (2006) 8703-8717.
[11] C. Schwieger, X. Liu, M.P. Krafft, Self-assembled mesoscopic surface domains of fluorocarbon–hydrocarbon diblocks can form at zero surface pressure: tilting of solid-like hydrocarbon moieties compensates for cross-section mismatch with fluorocarbon moieties, Phys. Chem. Chem. Phys. 19(35) (2017) 23809-23816.
[12] M. Veschgini, T. Habe, S. Mielke, S. Inoue, X.-H. Liu, M.P. Krafft, M. Tanaka, Existence of two-dimensional physical gels even at zero surface pressure at the air/water interface: Rheology of self assembled domains of small molecules, Angew. Chem. Int. Ed. 56 (2017) 12603–12607.
[13] L. Bardin, M.-C. Fauré, D. Limagne, C. Chevallard, O. Konovalov, E.J.M. Filipe, G. Waton, M.P. Krafft, M. Goldmann, P. Fontaine, Long-Range Nanometer-Scale Organization of Semifluorinated Alkane Monolayers at the Air/Water Interface, Langmuir 27(22) (2011) 13497-13505.
[14] M. Veschgini, W. Abuillan, S. Inoue, A. Yamamoto, S. Mielke, X.-H. Liu, O. Konovalov, M.P. Krafft, M. Tanaka, Size, shape, and lateral correlation of highly uniform, mesoscopic, self-assembled domains of fluorocarbon–hydrocarbon diblocks at the air/water interface: A GISAXS study, ChemPhysChem 18 (2017) 2791-2798.
[15] W. Abuillan, M. Veschgini, S. Mielke, A. Yamamoto, X. Liu, O. Konovalov, M.P. Krafft, M. Tanaka, Long-Range Lateral Correlation between Self-Assembled Domains of Fluorocarbon-Hydrocarbon Tetrablocks by Quantitative GISAXS, ChemPhysChem 20(6) (2019) 898-904.
[16] C. de Gracia Lux, J.-L. Gallani, G. Waton, M.P. Krafft, Compression of Self-Assembled Nano-Objects: 2D/3D Transitions in Films of (Perfluoroalkyl)Alkanes—Persistence of an Organized Array of Surface Micelles, Chem. Eur. J. 16(24) (2010) 7186-7198.
[17] C. de Gracia Lux, M.P. Krafft, Nonpolar gemini amphiphiles self-assemble into stacked layers of nano-objects, Chem. Eur. J. 16(38) (2010) 11539-11542.
[18] C. de Gracia Lux, J.-L. Gallani, G. Waton, P. Krafft Marie, Stacking of self-assembled surface micelles in ultrathin films, ChemPhysChem 13(6) (2012) 1454-1462.
[19] M.P. Krafft, J.G. Riess, Therapeutic oxygen delivery by perfluorocarbon-based colloids, Adv. Colloid Interface Sci. 294 (2021) 102407.

[20] J. Mackiewicz, K. Maaijwee, C. Lüke, N. Kociok, W. Hiebl, H. Meinert, A.M. Joussen, Effect of gravity in long-term vitreous tamponade: in vivo investigation using perfluorocarbon liquids and semi-fluorinated alkanes, Graefe's Arch. Clin. Exp. Ophthalmol. 245(5) (2007) 665-675.
[21] P. Steven, A.J. Augustin, G. Geerling, T. Kaercher, F. Kretz, K. Kunert, J. Menzel-Severing, N. Schrage, W. Schrems, S. Krösser, M. Beckert, E.M. Messmer, Semifluorinated alkane eye drops for treatment of dry eye disease due to Meibomian gland disease, J. Ocul. Pharm. Ther. 33 (2017) 678-685.
[22] J.G. Riess, Injectable oxygen carriers (blood substitutes) - Raison d'être, chemistry, and some physiology, Chem. Rev. 101(9) (2001) 2797-2920.
[23] S. Marie Bertilla, J.-L. Thomas, P. Marie, M.P. Krafft, Cosurfactant effect of a semifluorinated alkane at a fluorocarbon/water interface: Impact on the stabilization of fluorocarbon-in-water emulsions, Langmuir 20(10) (2004) 3920-3924.
[24] S. Audonnet-Blaise, M.-P. Krafft, Y. Smani, P.-M. Mertes, P.-Y. Marie, P. Labrude, D. Longrois, P. Menu, Resuscitation of severe but brief haemorrhagic shock with PFC in rabbits restores skeletal muscle oxygen delivery and does not alter skeletal muscle metabolism, Resuscitation 70(1) (2006) 124-132.
[25] J.G. Riess, Perfluorocarbon-based Oxygen Delivery, Artif. Cells, Blood Subst., Immob. Biotech. 34(6) (2006) 567-580.
[26] M. Sanchez Dominguez, E. Maillard, M.P. Krafft, S. Sigrist, A. Belcourt, Prevention of Adhesion and Promotion of Pseudoislets Formation from a β-Cell Line by Fluorocarbon Emulsions, ChemBioChem 7(8) (2006) 1160-1163.
[27] E. Maillard, M.T. Juszczak, A. Langlois, C. Kleiss, M.C. Sencier, W. Bietiger, M. Sanchez-Dominguez, M.P. Krafft, P.R.V. Johnson, M. Pinget, S. Sigrist, Perfluorocarbon Emulsions Prevent Hypoxia of Pancreatic β-Cells, Cell Transplant. 21(4) (2012) 657-669.
[28] C. Jacoby, S. Temme, F. Mayenfels, N. Benoit, M.P. Krafft, R. Schubert, J. Schrader, U. Flögel, Probing different perfluorocarbons for in vivo inflammation imaging by 19F MRI: image reconstruction, biological half-lives and sensitivity, NMR Biomed. 27 (2014) 261–271.
[29] I. Inci, S. Arni, I. Iskender, N. Citak, J.M. Rodriguez, M. Weisskopf, I. Opitz, W. Weder, T. Frauenfelder, M.P. Krafft, D.R. Spahn, Functional, Metabolic and Morphologic Results of Ex Vivo Donor Lung Perfusion with a Perfluorocarbon-Based Oxygen Carrier Nanoemulsion in a Large Animal Transplantation Model, Cells 9(11) (2020) 2501.
[30] R.H. Notter, Lung Surfactants: Basic Science and Clinical Applications, 1st Edition ed., CRC Press, Boca Raton, 2000.
[31] J. Pérez-Gil, Structure of pulmonary surfactant membranes and films: The role of proteins and lipid–protein interactions, Biochim. Biophys. Acta 1778(7) (2008) 1676-1695.
[32] Y.Y. Zuo, R.A.W. Veldhuizen, A.W. Neumann, N.O. Petersen, F. Possmayer, Current perspectives in pulmonary surfactant — Inhibition, enhancement and evaluation, Biochim.

Biophys. Acta 1778(10) (2008) 1947-1977.
[33] F. Gerber, M.P. Krafft, T.F. Vandamme, M. Goldmann, P. Fontaine, Preventing Crystallization of Phospholipids in Monolayers: A New Approach to Lung-Surfactant Therapy, Angew. Chem. Int. Ed. 44(18) (2005) 2749-2752.
[34] F. Gerber, M.P. Krafft, T.F. Vandamme, M. Goldmann, P. Fontaine, Fluidization of a dipalmitoyl phosphatidylcholine monolayer by fluorocarbon gases: potential use in lung surfactant therapy, Biophys. J. 90(9) (2006) 3184-3192.
[35] F. Gerber, M.P. Krafft, T.F. Vandamme, The detrimental effect of serum albumin on the re-spreading of a dipalmitoyl phosphatidylcholine Langmuir monolayer is counteracted by a fluorocarbon gas, Biochim. Biophys. Acta - Biomembranes 1768(3) (2007) 490-494.
[36] M.P. Krafft, Overcoming inactivation of the lung surfactant by serum proteins: a potential role for fluorocarbons?, Soft Matter 11(30) (2015) 5982-5994.
[37] H. Nakahara, S. Lee, M.P. Krafft, O. Shibata, Fluorocarbon-hybrid pulmonary surfactants for replacement therapy - a Langmuir monolayer study, Langmuir 26(23) (2010) 18256-18265.
[38] M.P. Krafft, F. Giulieri, P. Fontaine, M. Goldmann, Reversible stepwise formation of mono- and bilayers of a fluorocarbon/hydrocarbon diblock on top of a phospholipid Langmuir monolayer. A case of vertical phase separation, Langmuir 17(21) (2001) 6577-6584.
[39] M. Maaloum, P. Muller, M.P. Krafft, Lateral and Vertical Nanophase Separation in Langmuir-Blodgett Films of Phospholipids and Semifluorinated Alkanes, Langmuir 20(6) (2004) 2261-2264.
[40] M.F. Paige, A.a.F. Eftaiha, Phase-separated surfactant monolayers: Exploiting immiscibility of fluorocarbons and hydrocarbons to pattern interfaces, Adv. Colloid Interface Sci. 248 (2017) 129-146.
[41] H. Nakahara, M.P. Krafft, O. Shibata, How Self-Assembled Nanodomains Can Impact the Organization of a Phospholipid Monolayer-Flower-Like Arrays, ChemPhysChem 21(17) (2020) 1966-1970.
[42] S. Mielke, X. Liu, M.P. Krafft, M. Tanaka, Influence of Semifluorinated Alkane Surface Domains on Phase Behavior and Linear and Nonlinear Viscoelasticity of Phospholipid Monolayers, Langmuir 36(3) (2020) 781-788.
[43] F. Pan, Z. Lu, I. Tucker, S. Hosking, J. Petkov, J.R. Lu, Surface active complexes formed between keratin polypeptides and ionic surfactants, J. Colloid Interface Sci. 484 (2016) 125-134.
[44] N.O. Brace, Free-radical addition of iodoperfluoralkanes to terminal alkadienes. Relative reactivity as a function of chain length and reaction conditions, J. Org. Chem. 38(18) (1973) 3167-3172.
[45] H. Nakahara, M. Hagimori, T. Mukai, O. Shibata, Interactions of a tetrazine derivative with biomembrane constituents: A Langmuir monolayer study, Langmuir 32(26) (2016) 6591-6599.

[46] H. Nakahara, M. Hagimori, T. Mukai, O. Shibata, Monolayers of a tetrazine-containing gemini amphiphile: Interplays with biomembrane lipids, Colloids Surf. B: Biointerfaces 164 (2018) 1-10.
[47] S. Sakamoto, H. Nakahara, T. Uto, Y. Shoyama, O. Shibata, Investigation of interfacial behavior of glycyrrhizin with a lipid raft model via a Langmuir monolayer study, Biochim. Biophys. Acta 1828(4) (2013) 1271-1283.
[48] M. Broniatowski, I. Sandez Macho, J. Miñnes, Jr., P. Dynarowicz-Łatka, Langmuir Monolayers Characteristic of (Perfluorodecyl)-Alkanes, J. Phys. Chem. B 108(35) (2004) 13403-13411.
[49] P. Silva, D. Nova, M. Teixeira, V. Cardoso, P. Morgado, B. Nunes, R. Colaço, M.-C. Fauré, P. Fontaine, M. Goldmann, E.J.M. Filipe, Langmuir Films of Perfluorinated Fatty Alcohols: Evidence of Spontaneous Formation of Solid Aggregates at Zero Surface Pressure and Very Low Surface Density, Nanomaterials 10(11) (2020) 2257.
[50] H. Mohwald, Phospholipid and Phospholipid-Protein Monolayers at the Air/Water Interface, Ann. Rev. Phys. Chem. 41(Volume 41) (1990) 441-476.
[51] O.N. Oliveira, Jr., C. Bonardi, The Surface Potential of Langmuir Monolayers Revisited, Langmuir 13(22) (1997) 5920-5924.
[52] A. Gopal, K.Y.C. Lee, Headgroup Percolation and Collapse of Condensed Langmuir Monolayers, J. Phys. Chem. B 110(44) (2006) 22079-22087.
[53] P. Méléard, C. Gerbeaud, P. Bardusco, N. Jeandaine, M.D. Mitov, L. Fernandez-Puente, Mechanical properties of model membranes studied from shape transformations of giant vesicles, Biochimie 80(5) (1998) 401-413.
[54] H.M. McConnell, Structures and Transitions in Lipid Monolayers at the Air-Water Interface, Annu. Rev. Phys. Chem. 42(Volume 42) (1991) 171-195.
[55] D. Marsh, Lateral pressure in membranes, Biochim. Biophys. Acta - Reviews on Biomembranes 1286(3) (1996) 183-223.
[56] M.P. Krafft, J.G. Riess, Highly fluorinated amphiphiles and colloidal systems, and their applications in the biomedical field. A contribution, Biochimie 80(5) (1998) 489-514.
[57] A. Eftaiha, S.M.K. Brunet, M.F. Paige, Influence of film composition on the morphology, mechanical properties, and surfactant recovery of phase-separated phospholipid-perfluorinated fatty acid mixed monolayers, Langmuir 28 (2012) 15150-15159.
[58] A. Radhakrishnan, T.G. Anderson, H.M. McConnell, Condensed complexes, rafts, and the chemical activity of cholesterol in membranes, Proc. Natl. Acad. Sci. USA 97(23) (2000) 12422-12427.
[59] S. Trabelsi, S. Zhang, R. Lee, D.K. Schwartz, Linactants: Surfactant analogues in two dimensions, Phys. Rev. Lett. 100 (2008) 037802.